J. Hydrol. Hydromech., 70, 2022, 2, X–X
https://doi.org/10.2478/johh-2022-0001

sciendo Journal of Hydrology and Hydromechanics Institute of Hydrology SAS

Effects of carbonated water injection on the pore system of a carbonate rock (coquina)

Thaís M. Silveira[1], Fernanda Hoerlle[1], Adriano S. Rocha[1], Maira C.O Lima[1], Mateus G. Ramirez[2], Elizabeth M. Pontedeiro[1,3], Martinus Th. van Genuchten[3,4*], Daniel O.A. Cruz[2], Paulo Couto[1]

[1] Department of Civil Engineering, COPPE, Federal University of Rio de Janeiro, RJ, Brazil.
[2] Department of Mechanical Engineering, COPPE, Federal University of Rio de Janeiro, RJ, Brazil.
[3] Department of Earth Sciences, Utrecht University, Utrecht, Netherlands.
[4] Center for Environmental Studies, CEA, São Paulo State University, Rio Claro, SP, Brazil.
[*] Corresponding author. E-mail: rvangenuchten@hotmail.com

Abstract: CO_2 injection is a well-known Enhanced Oil Recovery (EOR) technique that has been used for years to improve oil extraction from carbonate rock and other oil reservoirs. Optimal functioning of CO_2 injection requires a thorough understanding of how this method affects the petrophysical properties of the rocks. We evaluated pore-scale changes in these properties, notably porosity and absolute permeability, following injection of CO_2-saturated water in two coquina outcrop samples from the Morro do Chaves Formation in Brazil. The coquinas are close analogues of Pre-salt oil reservoirs off the coast of southern Brazil. The effects of carbonated water injection were evaluated using a series of experimental and numerical steps before and after coreflooding: cleaning, basic petrophysics, microtomography (microCT) imaging, nuclear magnetic resonance (NMR) analyses, and pore network modeling (PNM). Our study was motivated by an earlier experiment which did not show the development of a wormhole in the center of the sample, with a concomitant increase in permeability of the coquina as often noted in the literature. We instead observed a substantial decrease in the absolute permeability (between 71 and 77%), but with little effect on the porosity and no wormhole formation. While all tests were carried out on both samples, here we present a comprehensive analysis for one of the samples to illustrate changes at the pore network level. Different techniques were used for the pore-scale analyses, including pore network modeling using PoreStudio, and software developed by the authors to enable a statistical analysis of the pore network. Results provided much insight in how injected carbonated water affects the pore network of carbonate rocks.

Keywords: Carbonate rocks; Coreflooding; Pore Size Distribution; Pore Network Analysis; PoreStudio.

INTRODUCTION

About 50 to 60% of the world's hydrocarbon reserves are contained in carbonate rocks (Akbar et al., 2000; Burchette, 2012; Mazzllo, 2004). CO_2 injection is a well-known Enhanced Oil Recovery (EOR) technique that has been used for years to improve oil recovery. A review of worldwide CO_2 flooding field projects indicates incremental recoveries ranging from 5 to 20% of the original oil in place (OOIP) (Sheng, 2013). Viscosity reductions and oil swelling are the main effects that enhance oil recovery, with wettability alterations and mineral dissolution also contributing to oil displacement (Drexler et al., 2019). CO_2 injection can cause dramatic changes in the fluid-fluid and rock-fluid interactions, such as reductions in the pH, reducing oil viscosity and enhanced rock dissolution. The resulting environment represents unique challenges in terms of wettability changes, thus adding uncertainties in fluid flow models (Wilson, 2014). Another major concern is that rock dissolution and precipitation resulting from CO_2-brine-rock interactions may affect the porosity and absolute permeability of oil reservoirs.

Carbonate dissolution depends not only on a range of fluid-related parameters such as temperature, salinity and fluid pressure, but also on configuration of the often highly heterogeneous pore system of carbonate rocks (Menke et al., 2016). Various studies demonstrated that during the dissolution of calcite a multitude of physical and geochemical processes occur at the pore scale. Modifications at the pore level and related porosity-permeability relations are a function of the initial heterogeneity and makeup of the rock, and of the specific dissolution conditions such as the injection rate and chemistry of the injected fluid (Golfier et al., 2002; Luquot et al., 2014; Molins et al., 2014).

No consensus exists in the literature if the porosity and permeability of carbonate rock samples increase or decrease when carbonated water imbibition experiments are carried out. Most studies indicate that core flooding with carbonated water leads to higher permeabilities, sometimes by creating a wormhole at and near the core entrance. For example, Nowrouzi et al. (2020) and Seyyedi et al. (2020) observed higher porosity and permeability values after injection. However, Drexler et al. (2019) noted a reduction in weight, porosity, pore volume and permeability of the sample after injecting carbonated water (desulphated seawater saturated with CO_2), while Abbaszadeh et al. (2016) reported a reduction in porosity and the sample's weight, but an increase in the permeability. By contrast, Wang et al. (2019) observed almost no changes in the porosity but a significantly lower permeability. Most studies noted the importance of rock dissolution as such, and the transport and deposition of fine particles (e.g., Jia, 2019; Mahzari et al., 2019). Grigg and Svec (2003), Drexler et al. (2019) and Mahzari et al. (2019) showed microCT images of a carbonate rock sample after injection of a brine rich in CO_2. While these studies observed localized calcite dissolution at the inlet of the sample, they did not explain the occurred phenomena at the pore scale.

Our own preliminary studies also did not show an increase in porosity, but instead pointed to a reduction in the permeability. This motivated us to carry out a detailed pore-scale study in order to understand the type of changes in the petrophysical properties that may occur at the pore scale. For this purpose, we used a combination of nuclear magnetic resonance (NMR) curves, microtomography (microCT) images, pore size distribution (PSD) analyses, pore network modeling (PNM) and statistical analyses before and after carbonated seawater (CSW) injection. The non-destructive microCT experiments were used to investigate changes in the internal pore structure of the samples to better understand permeability changes that may occur after carbonated water injection. X-ray microtomography is now widely used for both qualitative and quantitative pore-scale analyses, including for pore-scale flow modeling (Godoy et al., 2019; Lima et al., 2020; Saxena et al., 2017), determination of wettability through studies of the contact angle in images (Al Ratrout et al., 2018; Andrew et al., 2014; Armstrong et al., 2021; Prodanović et al., 2004), and analyses of the distribution of immiscible fluids inside pores (Alvarado et al., 2004; Schnaar and Brusseau, 2006), among other soil and rock hydrologic applications. MicroCT results provide input for digital pore and pore network modeling (PNM) analyses to highlight the pore-scale basis of macro-scale (or continuum-scale) multiphase fluid flow and contaminant transport processes (de Vries et al., 2017; Rabbani and Babaei, 2019; Raoof et al., 2013).

PNM approaches assume that the pore space can be approximated by a network (the skeleton) with a simplified geometry involving pore bodies connected by pore throats. A Eulerian description can then be used to obtain flow and contaminant transport properties of the medium. Despite being a simplified structure, the skeleton typically is composed by thousands of points, requiring statistical techniques for quantitative assessments, including how carbonated water injection may change the pore network. To estimate these changes, a set of analyses, referred to at Digital Pore Analysis (DPA), was developed as part of our study to characterize the pore network using averaged parameters. We note here that pore-scale models are not necessarily a substitute for experimental methods, but rather serve as a complement to better understand the experimental data and their uncertainties, and allowing one to replicate experimental conditions (Gundogar et al., 2016). In our study, calculations were carried out using the pore-scale network module within the PoreStudio software (PoreStudio website, 2021), which is an update of the PoreFlow model (Raoof et al., 2013) used by Raoof and Hassanizadeh (2012) and Godoy et al. (2019), among others.

The microCT results were used also as input for a digital pore-size distribution analysis to quantify the sum of volumes contained in different pore sizes. PSDs allow one to easily observe how much of the pore volume is contained within small, medium and large radii, thus allowing an assessment of the topology of the medium (Kantzas et al., 2012). These aspects are very relevant for our study in terms of understanding changes in the pore network due to CO_2 injection without adding extra modifications that may not be related to coreflooding. The PSD methodology used by Yang et al. (2009) allows estimation of the pore size distribution through high resolution images that preserve a dimensional equivalence between the pixel and the spacing between the different sections (Cássaro et al., 2017; Oliveira et al., 2020; Rocha et al., 2019). In our study we used the approach by Yang et al. (2009) to estimate PSDs before and after coreflooding.

We similarly used NMR techniques to indirectly estimate the PSDs through the excitation of nuclear spins, mainly ^1H contained in the saturating fluid molecules (e.g., Chi and Heidari, 2016; Lima et al., 2020). Typically, the pore distribution of a rock sample drives the distribution of transverse relaxation times (referred to as T_2), determined by mathematical inversion of relaxation measurements (Buttler et al., 1981). We note here that a constraint of the NMR approach (and resulting PSDs) concerns the bulk effect of the larger pores. Above 2.5 s (the saturating fluid relaxation time of the samples) the spins no longer completely collide with the pore walls of the pore network inside the sample, which may cause the measured relaxation times to be less reliable (Lima et al., 2020). This causes uncertainty in the size of especially the larger pores. The PSD analysis for this reason depends on the segmentation quality of the microCT stacks.

Specific objectives of our study were (1) to understand which part of the pore scale showed higher dissolution rates following carbonated water injection; (2) to evaluate changes in the pore system at the pore level (pore enhancements or possible obstructions/decreases) and (3) to verify and quantify the impact on permeability due to the changes in the pore-scale network.

MATERIALS AND METHODS

This section describes the various experimental tests, the numerical simulations, and other analyses that were carried out using the coquina samples. Fig. 1 provides a schematic of the workflow that was followed. Details of the various steps are provided below.

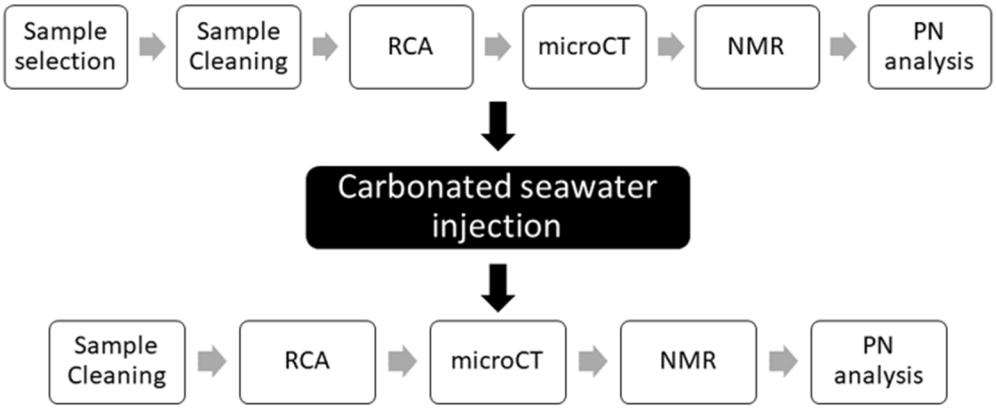

Fig. 1. Workflow used to guide the experiments and pore network analyses.

Carbonate rock samples

Since the 1970s, lacustrine carbonate reservoirs have been studied extensively in Brazil, prompted by significant pre-salt oil discoveries in ultra-deep offshore oil reservoirs of the Campos and Santos basins in southern Brazil (ANP, 2017; Corbett et al., 2017). Morro do Chaves Formation outcrops are considered to be close analogues of some facies in the Campos and Santos basins, and also in the Congo Basin of West Africa which contain coquinas of the same late Barremian early Aptian-Jiquiá age (Azambuja and Arieti, 1998; Corbett et al., 2016). The Morro do Chaves formation is part of the Sergipe-Alagoas basin in northeastern Brazil. The basin comprises a narrow strip between 20 and 50 km wide and 350 km long, covering parts of Sergipe and Alagoas states, as well as a small portion of Pernambuco, with one-third emerging and two-thirds being submerged up to a 3,000 m isobath (ANP, 2018).

Coquinas typically are composed by whole and fragmented shells, deposited by the actions of some transport agent (Schafer, 1972). The coquinas from Morro do Chaves Formation are formed by non-marine bivalves and ostracods, which lived in shallow oxygenated water, with their shells being re-transported, and deposited as wash-over fans and beaches that can show a strong storm influence and evidence of long-shore drift on low angle ramps (Thompson et al., 2015). Difficulty to access the offshore pre-salt rocks is a major reason for using analogues to improve studies of these types of rocks.

For our study we used two coquina samples taken from a block originating from the Atol Quarry, in São Miguel dos Campos (Fig. 2), belonging to the Morro do Chaves Formation. The two coquina plugs, MC1P3 and MC1P4, had a cylindrical shape, 5 cm in height and 2.5 cm in diameter. The samples had a light yellow color and had moderate grain selection, while their framework consisted of disarticulated bivalves (some of them partially fragmented) with granulometry ranging from very coarse sand to pebbles. Macroscopic descriptions and microCT analyses showed that the samples predominantly consisted of carbonate minerals without any siliciclastic minerals. The pores were visually classified as vug and moldic pores, with sizes ranging from 2 to 4 mm (Fig. 3A). Details of the top and base of the sample are also shown in Fig. 3.

Routine Core Analyses (RCA)

The samples were cleaned with toluene and methanol using the Soxhlet method. After cleaning, they were dried at a temperature of 60 °C for 24 h. The samples were characterized subsequently using routine petrophysics. For this step we used porosimeter-permeameter equipment to measure the porosity, pore volume, permeability, grain density, and total volume.

Fig. 2. Photograph of the Atol Quarry and detail of the front of the outcrop.

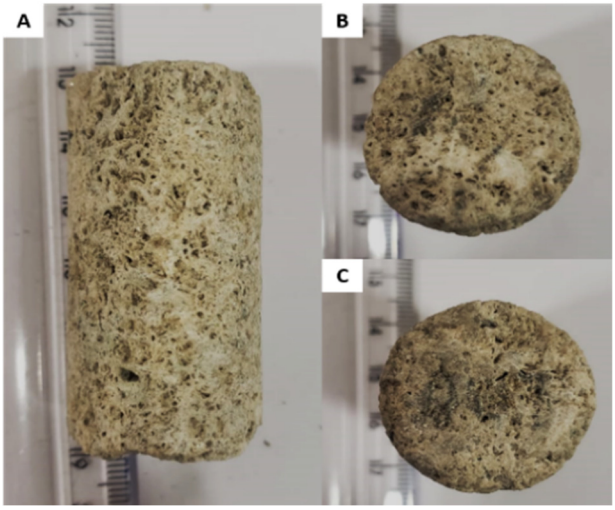

Fig. 3. Coquina sample from the Morro do Chaves Formation used in our study.

Nuclear magnetic resonance (NMR)

For the NMR analyses, the sample was placed in a saturator, subjected to vacuum for 8 h and then saturated with a 30,000 ppm KCl solution to minimize reactions of the clay material present into the pore space, at a constant pressure of 1,500 psi (10.34 MPa) for another 8 h. The NMR data were acquired in a low-field spectrometer Oxford Instruments equipment, model Geospec+ 12/53 3D imager. The samples for this purpose were wrapped with teflon tape to contain saturation throughout the experiment and positioned inside the probe. The CPMG pulse sequence was applied, and transversal relaxation measures (T_2) were obtained (Meiboom and Gill, 1958), from which the pore-size distribution was determined.

X-ray microtomography

The sample was imaged using a CoreTOM (Tescan/XRE) microCT system, before and after carbonated water injection, at a resolution of 15 µm. The equipment uses conical X-ray beam geometry, transmitted from the source, passing through the sample, and captured by a detector. At each step, a transmitted image is acquired and saved in 16-bit files (TIFF extensions). After acquisition, the images were reconstructed using the Acquila Reconstruction software (Tescan/XRE).

After the acquisition and reconstruction processes, the image sets were analyzed in two different ways: (1) using the Digital Pore Size Distribution program to obtain and evaluate the pore radius distribution before and after carbonated water injection, and (2) treating the image sets with the Avizo 9.5.0 software (2018) to generate the skeleton (to obtain information about the pore network), followed by a statistical analysis of the pore network and modeling flow in the sample using PNM techniques.

Coreflooding – CSW injection

The equipment used for carbonated seawater injection involved two Quizix pumps, a piston cell containing brine saturated with CO_2, a core holder, a back-pressure regulator (BPR), absolute pressure transducers, a gasometer, and a tube collector for the effluent fluids (Fig. 4). The test was performed on a benchtop at room temperature using an injection pressure of 10.34 MPa. The experiment proceeded by encapsulating and assembling the coquina rock sample inside the core holder. A confinement pressure of 500 psi (3.45 MPa) was applied. With the sample inside the holder, vacuum was applied for 8 h, after which the sample was saturated with formation brine at a constant injection pressure of 100 psi (0.69 MPa). Fluid used for this procedure was synthetic formation water (FW) from a Brazilian pre-salt field. The complex brine fluid had a high salinity (approximately 235,000 ppm total dissolved solids) as shown in Table 1.

To prepare the CSW, desulphated seawater (DSW) was fully saturated with CO_2 (Table 1). This recombination was done at room temperature and a pressure of 500 psi (10.34 MPa). For this process we used 1,000 mL of DSW and injected 51.68 mL of CO_2 into the brine to make it supersaturated with CO_2. Five pore volumes of CSW were subsequently injected into the sample at a constant flow rate of 50 cm³/h. A bump flow of 100 cm³/h was used to reduce any edge effects of the injection into a small sample. One pore volume of CSW was injected during the bump flow.

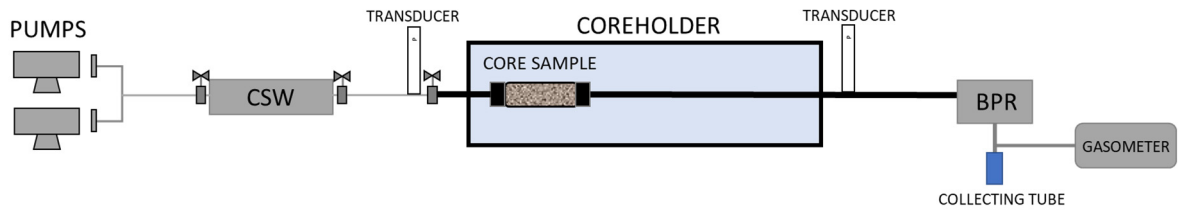

Fig. 4. Diagram of the benchtop apparatus used for the carbonated sea water (CSW) flooding tests (drawing is not to scale; BPR denotes the back-pressure regulator).

Table 1. Fluid data of synthetic pre-salt formation water (FW) and desulfated seawater (DSW) used for the coreflooding experiments. Ion concentrations are in ppm.

Ions	FW	DSW
Na^+	56,489	12,000
Ca^{2+}	22,290	500
Mg^{2+}	4,035	1,700
K^+	2,803	500
Ba^{2+}	391	0
Sr^{2+}	4,491	9
SO_4^{2-}	0	0
Cl^-	144,510	21,347
HCO_3^-	0	101
CO_3^-	0	31
Acetate	121	0
Li	102	0
TDS (ppm)	236,009	36,188
pH at 25 °C	5.94	8.85
ρ (g/mL) at 25 °C and 0.0101 MPa	1.16	1.01
CO_2 solubility at 60 °C and 10.34 MPa (mol%)	–	1.40

RESULTS AND DISCUSSION

Routine Petrophysics

Results of the routine petrophysics measurements for the two coquina samples (MC1P3 and MC1P4) before and after CSW injection are shown in Table 2. Measurements included pore volume, porosity, absolute permeability, and grain density. As can be seen from the routine petrophysical data, the CSW reacted with the sample and modified their pore system. Both samples did not show any changes in their length, diameter, and grain density. We observed slight reductions (about 2%) in the dry weight of the samples: 1.4 g for MC1P3 and 0.73 g for MC1P4, which may have been due to loss of grain during removal of the core holder or due to grain dissolution following reactions of CO_2 with the rock sample. Reductions in the porosity and pore volume of both samples were found to be very small: 0.04% and 0.15 cm³, respectively, for MC1P3, and 0.85% and 0.07 cm³, respectively, for sample MC1P4, perhaps simply related to equipment errors and/or slight grain removal. However, the permeability was reduced drastically in both samples due to CO_2 reactions with the carbonate rock. For sample MC1P3 the permeability went from 2,336 mD to 543 mD, a reduction of 1,793 mD (77%), while sample MC1P4 had its permeability reduced from 1,325 mD to 384 mD, a total reduction of 941 mD (71%). Given these drastic changes in the routine petrophysical data, we found it necessary to investigate more carefully the reasons for the reductions in the permeability, but maintenance of the sample porosity. Since the samples showed similar responses to the coreflooding experiment, we subjected sample MC1P4 to a series of tests (such as NMR, microCT, PNM and Digital Pore Analysis) to analyze the pore system at the microscale and understand what happened with the coquinas after the injection of carbonated water.

Nuclear magnetic resonance

NMR results of sample MC1P4 before and after carbonated water injection are presented in Fig. 5. The two curves have the same relaxation peak at 1000 ms, indicating a relatively large volume of macropores (Ramamoorthy et al., 2008). We could not determine which part of the pore system dissolved or was subject to clogging. Thus, the NMR results showed a need for more detailed study using microCT.

Pore size distributions

The incremental PSDs of sample MC1P4 before and after CSW injection obtained from the microCT images are presented in Fig. 6. The curves show incremental porosities between 15 and 735 µm, using a spacing of 30 µm between consecutive diameters. Fig. 7 shows a plot of incremental porosity changes, $\Delta\phi_{incr}$, in the pore size distribution before and after coreflooding, while Fig. 8 shows the cumulative porosity (being the sum of the incremental porosities in increasing order of pore diameter). The three figures indicate that carbonated water injection considerably altered the pore microstructure of the sample, leading to much lower fluid flow properties of the pore systems as will be shown later. One initial indication was the slight decrease in digital porosity, which reduced minimally from 14% to 13.8%, but involved a difference of more than 3 million pore pixels. While a lower porosity does not necessarily cause a

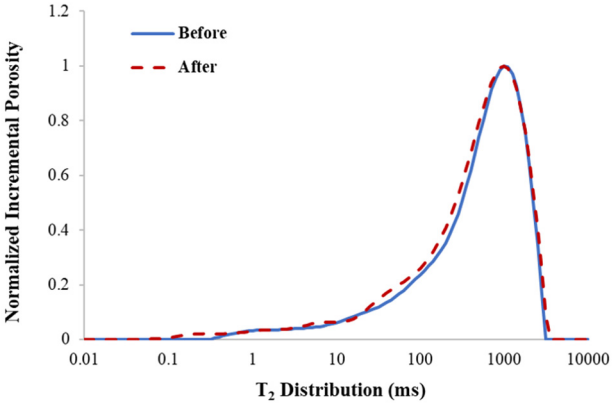

Fig. 5. NMR curves of sample MC1P4 before and after the EOR test.

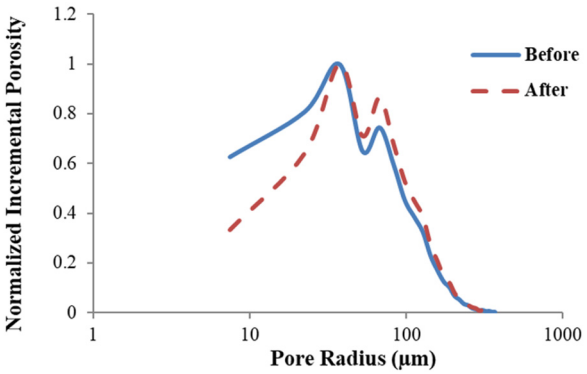

Fig. 6. Digital pore size distributions before and after coreflooding.

Table 2. Routine petrophysics of the MC1P3 and MC1P4 coquina samples before and after carbonated water injection.

SAMPLES PROPERTIES	MC1P3		MC1P4	
	Before	After	Before	After
Dry weight (g)	66.2	64.8	51.5	50.8
Length (cm)	6.72		5.04	
Diameter (cm)	2.47		2.47	
Grain density (g/cm³)	2.71		2.71	
Porosity (%)	22.3	22.3	19.8	18.9
Pore volume (cm³)	7.0	6.9	4.7	4.6
Permeability (mD)	2,336	543	1,325	384

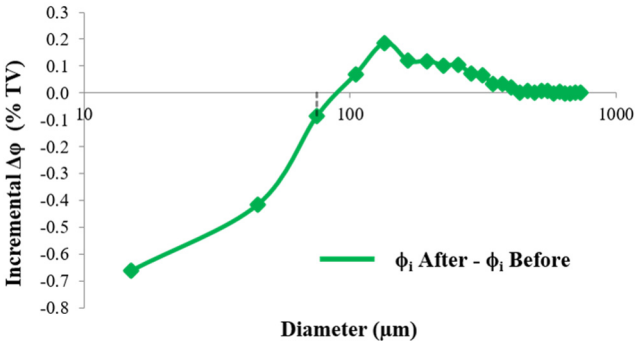

Fig. 7. Digital incremental porosity variation after coreflooding.

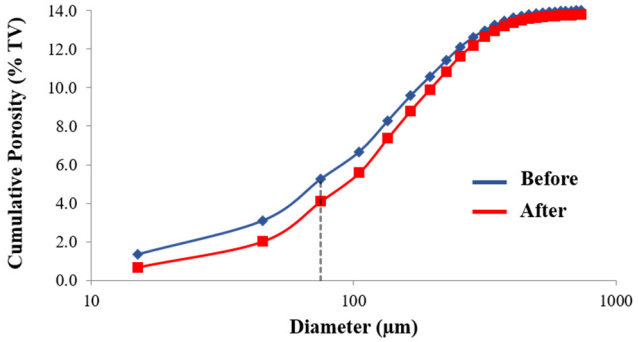

Fig. 8. Cumulative porosity distributions before and after coreflooding.

lower permeability, the slightly lower porosity after coreflooding suggests some particle deposition and possible restrictions in the connectivity of the pore network. These effects should have far greater potential for reducing the permeability due to restricted connections between the pore bodies and pore throats.

A second indication of the decrease in permeability is a reduction in the pore volumes associated with the smaller pores, which generally characterize the pore throats. The incremental porosity of the smaller diameters (from 15 µm to 75 µm) decreased significantly, while the incremental porosity of diameters greater than 75 µm increased slightly (Figs. 6 and 7).

The joint analysis of the diameters that make up the regions of loss or gain in pore volume showed that the total volume reduction of pores having the three smallest diameters (of 15, 45 and 75 µm) exceeded the total gain of pore volume of the larger diameters, with the overall difference producing a slight decrease in the digital porosity before and after CSW injection (0.21% of the sample volume). This shows that the reduction in digital porosity is due to a loss of pore volume of pores having the smallest diameters, with important consequences in terms of the permeability by affecting the pore network connectivity. In other words, material resulting from dissolution processes in regions with the larger pores seem to move within the pore network to cause obstructions in or between the pore throats, thus reducing the connected clusters. These results are consistent with those by Yang et al. (2009), who noted that the particle precipitation process depends on pore size, with precipitation more likely to increase as the pore diameter decreases. We conclude from the PSD analysis that dissolution of part of the pores may have caused a loss of connectivity of the pore network, leading to a reduction in flow and consequently a lower absolute permeability.

Since the sample porosity calculated using routine core analysis was 19.8% before coreflooding, we estimate that the digital model was able to identify about 70% of the pore volume, with the remaining 30% being in the region of pores having diameters below the image resolution of 15 µm. One possible hypothesis hence is that these pores with diameters in the microporosity and sub-resolution range (which likely are most susceptible to particle deposition and clogging), are partly responsible for reducing the permeability of the sample. Even though the proportion of larger pores increased as a result of carbonated seawater injection, deposition of rock material occurred in the smaller pores (mostly the throats), with considerable impact on the permeability while only slightly changing the overall sample porosity.

MicroCT analysis

After processing a microCT stack image of the sample, the pores were segmented from which the visible porosity in the resolution could be estimated. With the segmented pores, the skeleton of the image could be constructed. At this stage, the incremental pore volume changes in Fig. 7 could be confirmed by the main percolation clusters in the coquina (Fig. 9) before and after CSW injection (Godoy et al., 2019; Hoerlle et al., 2020; Lima et al., 2020). A more detailed evaluation is presented in the following section based on the generated skeleton of the sample. In this step, the pore space was transformed into cylindrical tubes (equivalent to the pore throats) and spheres (the pore bodies). As output, the Avizo software provided a spreadsheet with the skeleton topology comprising the nodes (the pore bodies and their connectivity), the points (all pores with their location and radius) and segments (sequence of pores forming the throats) of all connected clusters. These data were used to prepare the necessary input data for modeling at the pore level using PoreStudio.

Digital pore analysis

This section discusses the changes that occurred within the MC1P4 sample due to coreflooding, using a set of digital techniques we developed and further referred to as the Digital Pore Analysis (DPA). The analysis comprised statistical evaluations of relevant parameters using an in-house DPA program, as well as pore network flow modeling using PoreStudio, based on skeletons obtained from the microCT images and processed using the Avizo 9.5 software. Numerical results and 2D flow graphs generated with the PoreStudio software were supplemented with 3D images using the Paraview software (2020). This allowed a detailed numerical/visual analysis of changes in the pore system. Results for the MC1P4 pore system as obtained with the DPA statistical software and the pore network modeling are described below.

Statistical evaluation at the pore level

Using the skeletons as generated from the microCT images, we characterized the pore structure of the carbonate rock, before and after CSW injection, and provided a quantitative analysis of in terms of global parameters, the PSD, and variations of several properties in different sections of the MC1P4 rock sample.

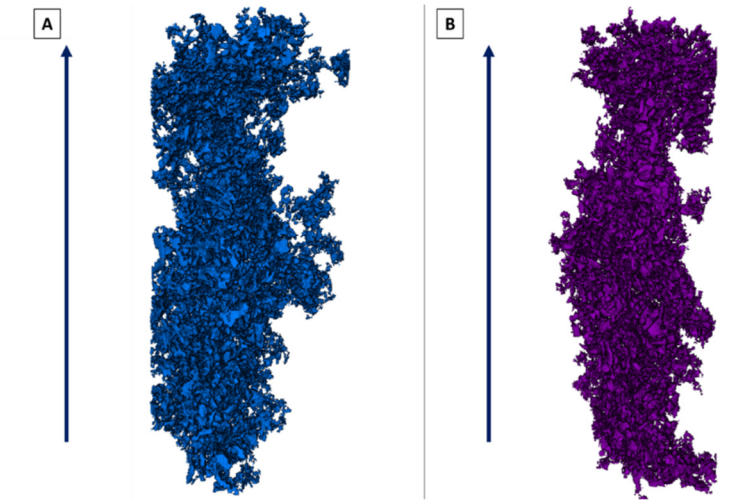

Fig. 9. Images showing the main pore clusters of sample MC1P4 before (A) and after (B) carbonated water injection. The vertical arrows indicate the Z axis.

Table 3. Global characteristics of the pore network of sample MC1P4 before and after carbonated water injection.

Characteristic	Before	After	Variation (%)
Digital connected porosity (%)	15.05	9.24	–38.6
Pores	407,049	234,757	–42.3
Throats	537,681	308,977	–42.5
Average connectivity	2.64	2.63	–0.4

Global parameters

The first properties to be evaluated are global parameters, notably porosity, number of the pore bodies and pore throats, and pore connectivity, as summarized in Table 3. A quantitative comparison of the pore structure before and after CSW injection indicated a considerable reduction in the pore volume of the skeleton (43.54%), which agreed well with the visual comparisons in Figs. 9A and B showing a higher concentration of points before injection. The reduction in porosity is also accompanied by a decrease in the number of pores (42.3%) and throats (42.5%), thus giving a first indication of why the permeability changed so dramatically. The average connectivity was also estimated. However, since sample MC1P4 had only a very small change in connectivity (0.36%), one must analyze this result together with the other DPA results to understand how the test affected the pore network. This is detailed further below.

Pore size distributions

To better understand the pore structure and why the connectivity reduced, even if only 0.4%, a DPA analysis of the skeleton was performed to determine the contribution of sets of pores to the porosity as a function of the radius size (the incremental porosity). This analysis is similar as carried out earlier using images instead of the skeleton. The current analysis was done by separating the pore body and pore throat contributions to the pore volume, based on the radii. Resulting graphs of the pore body and pore throat volumes versus pore radius are shown in Figs. 10 and 11, respectively.

Figs. 10 and 11 show that the reduction in the porosity is well represented by the loss of volume, both in the pore bodies and pore throats, with concomitant reductions in the overall distributions, especially for the larger pores. In addition to the variations for the larger pores, another important point in Fig. 10 is that pores with radii larger than about 28 pixels (420 μm) no longer are present in the digital structure, which suggests that pores originally above that radius have been partially or wholly filled and/or may have become completely isolated and removed from the connected pore network. When analyzing the PSD data in the previous section, it seems that part of the larger pores was excluded from the connected pore network. This then resulted in a lower connected porosity, indicating the existence of a disconnected region containing some of the larger pores.

Longitudinal partitioning

After evaluating the pore distribution, we performed a DPA analysis that digitally divided the 5.04 cm long sample into 20 cylindrical sections, each having the same length of about 0.25 cm and the same diameter as the original sample (2.47 cm). We used this method to better understand variations in the pore structure throughout the rock sample by characterizing porosity, the quantity and size of pores, the tortuosity and possible constrictions.

Fig. 12 shows the pore network by section along the sample before and after the coreflooding experiment. The data indicate that the number of pore bodies and pore throats are almost identical throughout the sample, which suggests that coreflooding seems to have affected both pore types equally in each section (Figs. 12B, C). Also, the variations in porosity do not seem to be linked mainly to variations in the number of pore bodies and throats, as can be seen by the mismatch of the frequency and porosity variations in Fig. 12C. This finding is noteworthy because variations in porosity (Fig. 12A) seem to be due mainly to other parameters of the porous medium, a hypothesis confirmed by the data in Fig. 13, which indicate that the mean pore radius indeed had a greater influence.

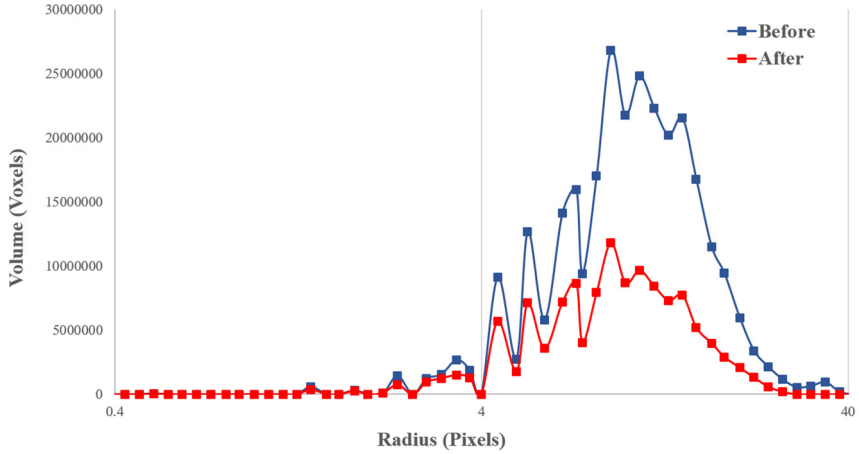

Fig. 10. Pore body volume distributions obtained from the skeleton data of sample MC1P4 before and after the carbonated water injection test.

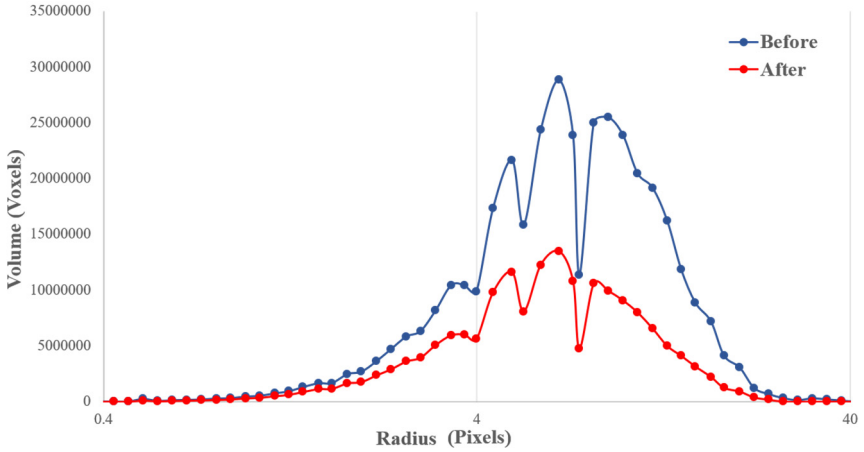

Fig. 11. Pore throat volume distributions obtained from the skeleton data of sample MC1P4 before and after the carbonated water injection test.

The distributions in Fig. 13 show that the pore network changes following CSW injection are linked mainly with changes in the size of the radii of the pore bodies and especially the pore throats, but not the pore lengths. The data in Fig. 13C seem to suggest some dissolution near the entrance and deposition in different sections along the sample, as shown also by the porosity graph in Fig. 12A.

The analysis above indicates that changes occurred in the pore network, with non-uniform dissolution and deposition in the different sections along the rock sample. This may have contributed to completely or partially isolating/filling pores and throats, as demonstrated by the changes in the pore distribution and reductions in the mean radii. In addition to creating an erosion/deposition system between sections, this effect may have been responsible for reducing the connected porosity visible in the tomography images, from 20% before injection to 11% after injection. Partial filling of the smaller pores may have caused them to be isolated from connected porosity and/or to reach sub-resolution diameters which no longer could be detected with the 15 μm imaging resolution of our microCT study.

Pore network modeling

This part of the research uses the skeletons generated before and after the coreflooding test. The flux in the connected part of the skeleton was calculated using the PNM module of the PoreStudio (2021) software. We used the Single Phase module within PoreStudio to obtain the pressure distributions inside the sample and the resulting tridimensional flux, and from these data the permeability and connected porosity. Table 4 provides the pore network characteristics of sample MC1P4. The data indicate that the permeability, and the number of pore bodies and pore throats, diminished after the experiment. We observed a volume decrease in the diameters of all pore bodies and pore throats (micro, meso and macro). On the other hand, there was an increase in the number of throats that did not participate in the flow processes (inactive throats, including those connected to isolated pore bodies) after CSW injection.

One advantage of using skeletons is to be able to visually compare the generated images using the Paraview software. The images in Fig. 14 show changes at the pore level after the injection of carbonated water. Shown are the connected pore bodies and pore throats of the pore network before (A) and after (B) the coreflooding test, with pore bodies represented by spheres (black) and the throats by cylinders (colored). Figs. 14C and 14D (before and after coreflooding) show the main percolation clusters (dark grey) and the disconnected clusters which did not contribute to the flux (in yellow). One can see a clear reduction in the size of the pore bodies and throats in Fig. 14B (after injection) and an increase in the number and size of disconnected groups (14D). The image before the injection contained 69 percolation clusters, while we obtained 214 separate percolation clusters after injection, with most of the latter clusters not being very extensive.

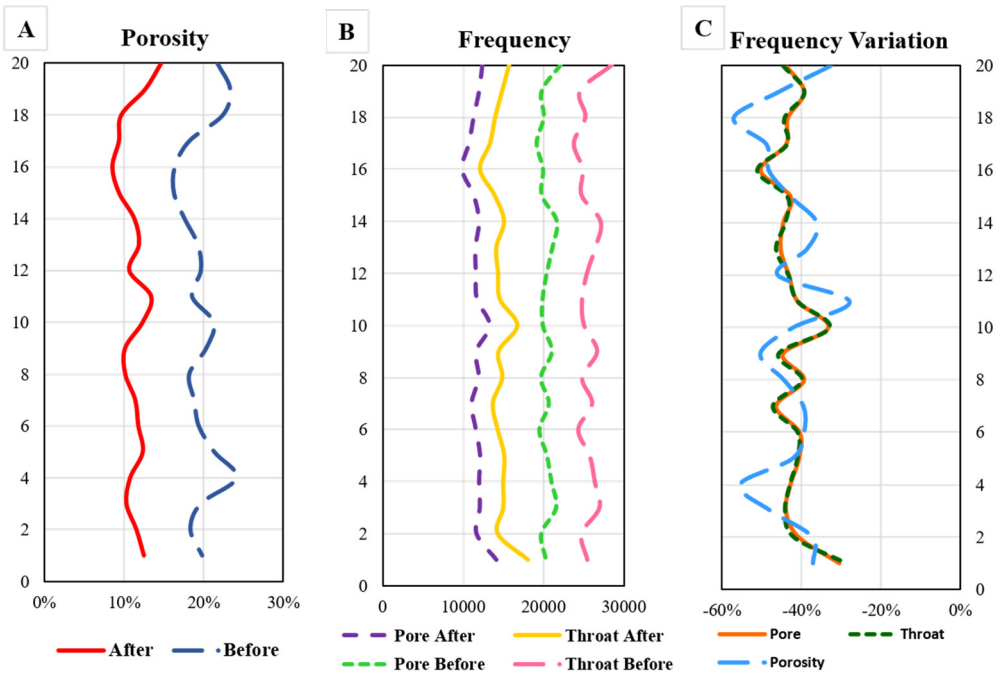

Fig. 12. Graphs of (A) the porosity, (B) the number of pore bodies and pore throats, and (C) changes in the porosity and number of pore bodies/throats in the plug sections before and after carbonated water injection.

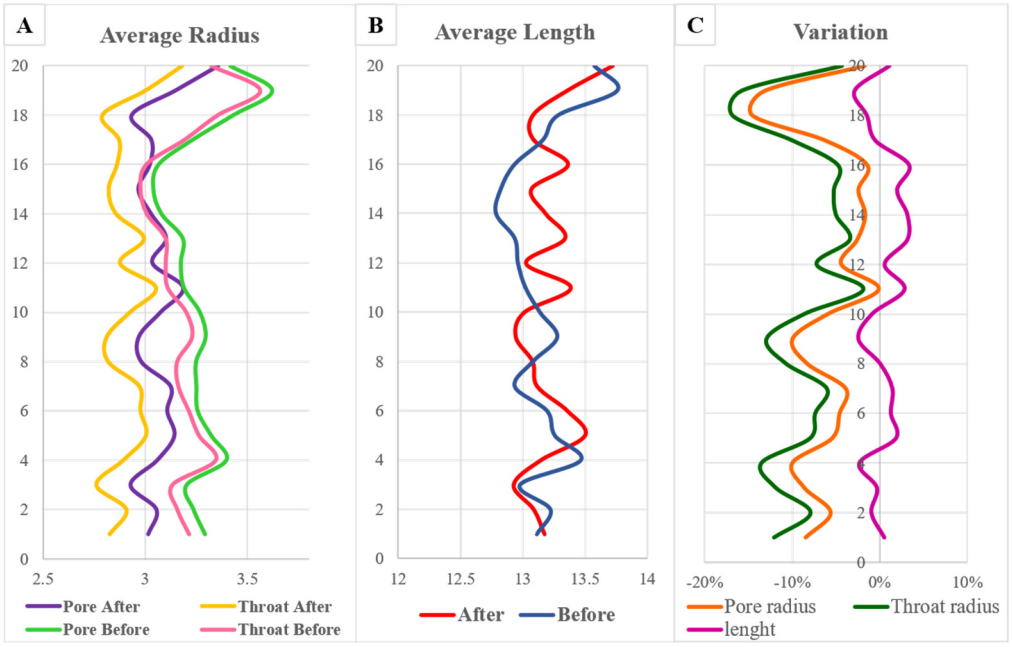

Fig. 13. Graphs of (A) average pore body and throat radii, (B) pore throat lengths, and (C) changes in the pore bodies and pore throat radii and the pore throath length in the plug sections before and after carbonated water injection.

Table 4. Percolation characteristics based on the microCT skeleton of sample MC1P4 before and after carbonated water injection.

Characteristics	Before	After	Variation (%)
Permeability (mD)	1,245	358	–71
Throat volume (mm^3)	1,244	677	–46
Micro throats volume (mm^3)	105.6	67.4	–36
Meso/macro throat volume (mm^3)	1,139	610	–46
Pore volume (mm^3)	968	414	–57
Micro pore volume (mm^3)	8.30	5.23	–37
Meso/macro pore volume (mm^3)	960	408	–58
Inactive throats	24	476	1,883
Isolated pores	1,698	4289	153

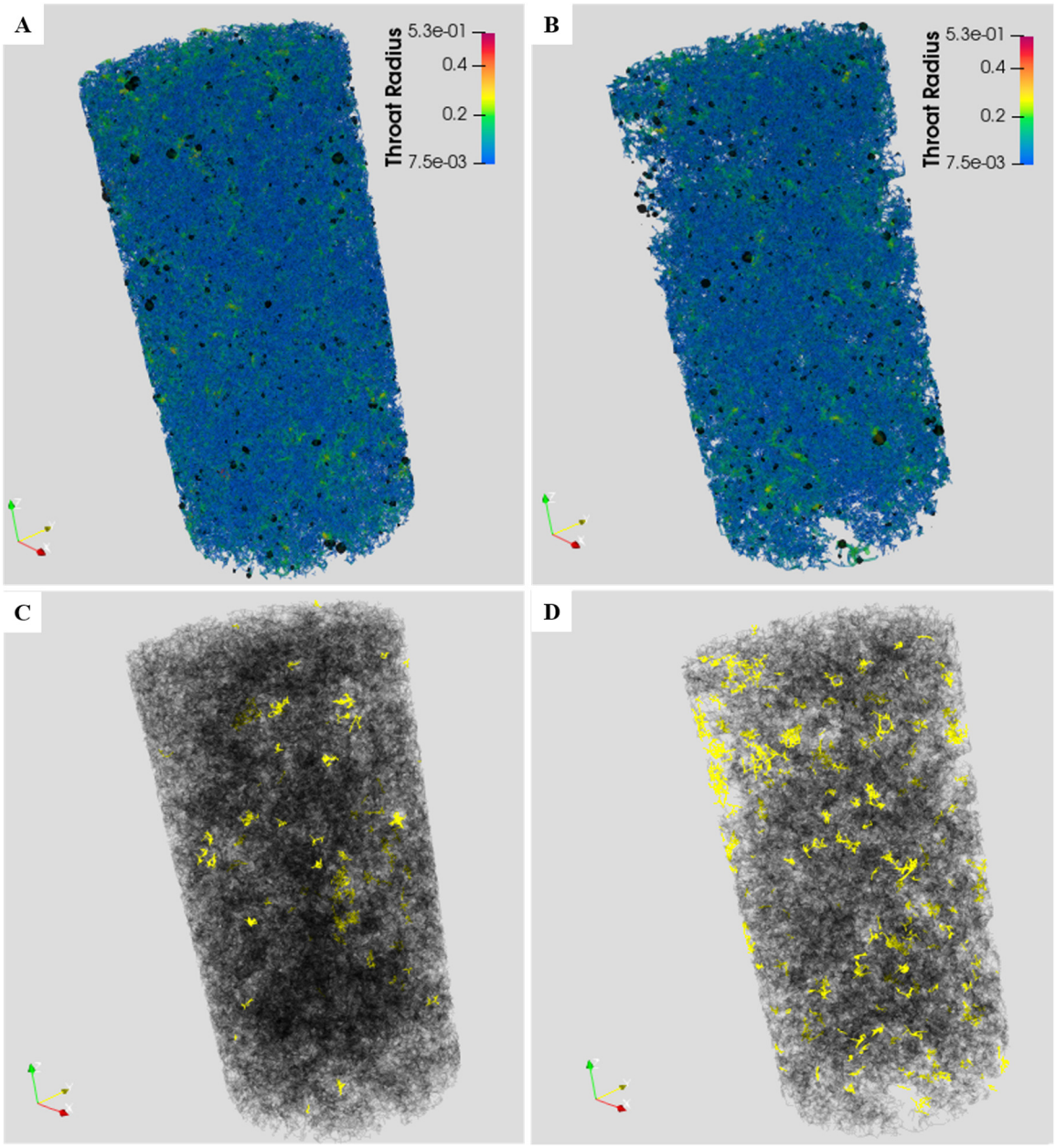

Fig. 14. Distributions of connected pore bodies (in black) and pore throats (colored) of sample MC1P4 before (A) and after (B) carbonated water injection. Also shown are the percolating clusters (dark grey) and disconnected clusters (in yellow) of pore bodies and throats before (C) and after (D) injection.

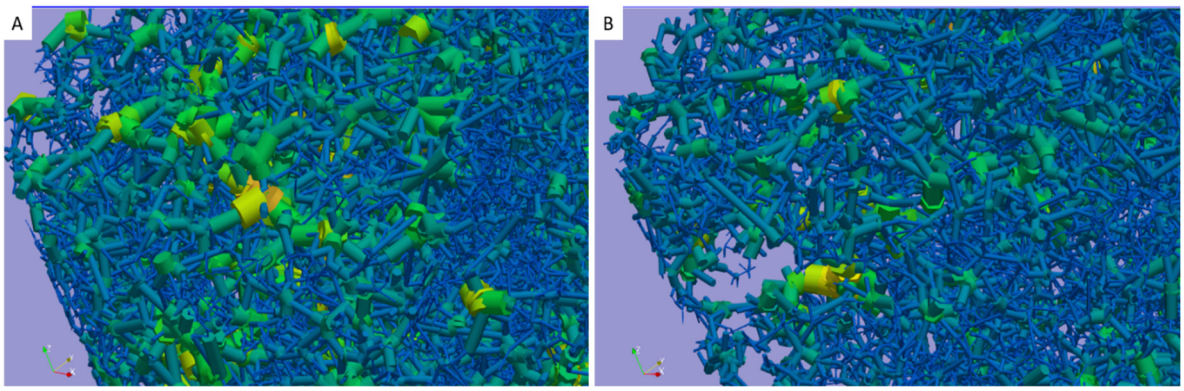

Fig. 15. Details of the sample top (A) before and (B) after the coreflooding test.

Fig. 15 provides in more detail a zoom of the top part of the coquina (sample MC1P4) as modeled using PoreStudio, again before and after coreflooding. It is possible to notice a much denser pore network in Fig. 15A (before injection), with bigger

pore bodies and more throats. The throat radius varied from 7.5 to 527 μm, with the smaller radii represented by blue tubes and the bigger radii by yellow tubes. The pore network in Fig. 15B (image after injection) shows some empty areas, which reflect less dense local networks, and also a reduction in the throats/pore body radii (varying between 7.5 and 373 μm).

CONCLUSIONS

This research presents a detailed analysis of changes in the pore network of an outcrop carbonate rock sample (coquina) from the Morro do Chaves Formation in Brazil, subjected to carbonated seawater injection in a coreflooding bench apparatus. Instead of observing the formation of a preferential flow path (such as a wormhole) or higher permeabilities as often reported in the literature for other types of rocks, we observed experimentally a drastic decrease in the permeability, with the porosity remaining essentially the same. Many previous studies focused on the possible formation of wormholes (enhanced permeabilities) or the causes of rock dissolution. Our objective was to analyze changes in the pore network in more detail to better understand why very small changes in the porosity could lead to substantial changes in the permeability. We postulate that some dissolved material from areas near the entrance of the carbonate rock sample migrated and partially or even totally blocked some of the pores (especially the pore throats and smaller pores) in the sample. Areas containing meso and macropores were found to have a slight increase in their radii, which did provide enough dissolved solid material to partially or entirely filling micropores. Although carbonated water injection reduced the total porosity by only 2%, the absolute permeability decreased by more than 70%. This decrease in permeability was first measured experimentally using routine petrophysical analyses, and then studied in detail at the pore scale using microCT images, pore network modeling, digital pore size distributions, and digital pore network analyses. Results leads us to deduce that a good part of the connectivity of the porous medium was governed by throats with relatively smaller radii, and that these throats were compromised or even removed from the percolation network after contact with water saturated with CO_2. The use of different tools to analyze the pore networks before and after the coreflooding test, and to quantify network changes that occurred, improved our overall view of the changes that may occur when carbonated seawater is injected in carbonate rocks, or other media, to improve EOR techniques or other applications such as CO_2 sequestration.

Acknowledgements. This research was carried out in association with ongoing R&D projects registered as ANP 19027-2, “Desenvolvimento de infraestrutura para pesquisa e desenvolvimento em recuperação avançada de óleo – EOR no Brasil” (UFRJ/Shell Brasil/ ANP) setting-up a advanced EOR Lab facility for R&D in Brasil, and ANP 20163-2, “Análise experimental da recuperação de petróleo para as rochas carbonáticas do pré-sal brasileiro através da injeção alternada de CO_2 e água”, sponsored by Shell Brasil under the ANP R&D levy as “Compromisso de Investimentos com Pesquisa e Desenvolvimento”. This study was financed in part by the Coordenação de Aperfeiçoamento de Pessoal de Nível Superior- Brasil (CAPES) - Finance Code 001, and carried out with the support of CNPq (National Council of Scientific and Technological Development, Brazil). We also thank the research teams of LRAP/COPPE/UFRJ.

REFERENCES

Abbaszadeh, M., Nasiri, M., Riazi, M., 2016. Experimental investigation of the impact of rock dissolution on carbonate rock properties in the presence of carbonated water. Env. Earth Sci., 75, 9, 791.

Al Ratrout, A., Blunt, M.J., Bijeljic, B., 2018. Wettability in complex porous materials, the mixed-wet state, and its relationship to surface roughness. Proc. Natl. Acad. Sci., 115, 8901–8906. DOI: 10.1073/pnas.1803734115

Alvarado, F.E., Grader, A.S., Karacan, O., 2004. Visualization of three phases in porous media using micro computed tomography. Petrophysics, 45, 6, 490–498.

Andrew, M., Bijeljic, B., Blunt, M.J., 2014. Pore-scale contact angle measurements at reservoir conditions using X-ray microtomography Adv. Water Resour., 68, 24–31. https://doi.org/10.1016/j.advwatres.2014.02.014

ANP, 2017. http://geofisicabrasil.com/noticias/55-governo21/870-anp-segundo-poco-tao-grande-quanto-primeiro.html

ANP, 2018. Agência Nacional do Petróleo, Gás Natural e Biocombustíveis. Anuário estatístico brasileiro do petróleo, gás natural e biocombustíveis. http://www.anp.gov.br/publicacoes/anuario-estatistico/anuario-estatistico-2018

Armstrong, R.T., Sun, C., Mostaghimi, P., Berg, S., Rücker, M., Luckham, P., Georgiadis, A., McClure, J.A., 2021. Multiscale characterization of wettability in porous media. Transp. Porous Media, 140, 1, 215–240. https://doi.org/10.1007/s11242-021-01615-0

Azambuja, N.C., Arienti, L.M., 1998. Guidebook to the Rift-Drift Sergipe-Alagoas, Passive Margin Basin, Brazil. The 1998 Am. Assoc. Petrol. Geol. Int. Conf. and Exhib.

Avizo, 2018. Avizo version 9.5.0. Thermo Fisher Scientific, Berlin.

Akbar, M., Vissapragada, B., Alghamdi, A.H., Allen, D., Herron, M., Carnegie, A., Dutta, D., Olesen, J-R., Chourasiya, R.D., Logan, D., Stief, D., Netherwood, R., Russell, S.D., Saxena, K., 2000. A snapshot of carbonate reservoir evaluation. Oilfield Rev., 12, 4, 20–21.

Burchette, T.P., 2012. Carbonate rocks and petroleum reservoirs: a geological perspective from the industry. Geological Society, London, Special Publications, 370, 1, 17–37.

Buttler, J.P., Reeds, J.A., Dawson, S.V., 1981. Estimating solution of first kind integral equations with non-negative constraints and optimal smoothing. SIAM J. Num. Anal., 18, 3, 381–397. https://doi.org/10.1137/0718025

Cássaro, F.A.M., Durand, A.N.P., Gimenez, D., Vaz, C.M.P., 2017. Pore-size distributions of soils derived using a geometrical approach and multiple resolution microCT images. Soil Sci. Soc. Am. J., 81, 3, 468–476.

Chi, L., Heidari, Z., 2016. Directional-permeability assessment in formations with complex pore geometry with a new NMR based permeability model. Soc. Petr. Eng. J., 21, 4, 1436–1449.

Corbett, P.W.M., Estrella, R., Rodriguez, A.M., Shoeir, A., Borghi, L.F., Tavares, A.C., 2016. Integration of Cretaceous Morro do Chaves rock properties (NE Brazil) with the Holocene Hamelin Coquina architecture (Shark Bay, Western Australia) to model effective permeability. Petr. Geosci., 22, 2, 105–122.

Corbett, P.W.M., Wang, H., Câmara, R.N., Tavares, A.C., Borghi, L.F., Perosi, F., Machado, A., Jiang, Z., Ma, J., Bagueria, R., 2017. Using the porosity exponent (m) and pore-scale resistivity modelling to understand pore fabric types in coquinas (Barremian-Aptian) of the Morro do Chaves Formation, NE Brazil. Marine Petrol. Geol., 88, 628–647.

de Vries, E.T., Raoof, A., van Genuchten, M.Th., 2017. Multiscale modelling of dual-porosity media: a computational pore-scale study flow and solute transport. Adv. Water Re-

sour., 105, 82–95. DOI: 10.1016/j.advwatres.2017.04.013
Drexler, S., Silveira, T.M., De Belli, G., Couto, P., 2019. Experimental study of the effect of carbonated brine on wettability and oil displacement for EOR application in the Brazilian Pre-Salt reservoirs. In: Energy Sources. Part A: Recovery, Utilization, and Environmental Effects, pp. 1–15.
Godoy, W., Pontedeiro, E.M., Hoerlle, F., Raoof, A., van Genuchten, M.Th., Santiago, J., Couto, P., 2019. Computational and experimental pore-scale studies of a carbonate rock sample. J. Hydrol. Hydromech., 67, 4, 372–383. DOI: 10.2478/johh-2019-0009
Golfier, F., Zarcone, C., Bazin, B., Lenormand, R., Lasseux, D., Quintard, M., 2002. On the ability of a Darcy-scale model to capture wormhole formation during the dissolution of a porous medium. J. Fluid Mech., 457, 213–254. DOI: 10.1017/S002211200 2007735
Grigg, R.B., Svec, R.K., 2003. Co-injected CO2-brine interactions with Indiana Limestone. In: Proc. SCA2003-19 Int Symp. Society of Core Analysts, Pau, France.
Gundogar, A.S., Ross, C.M., Akin, S., Kovscek, A.R., 2016. Multiscale pore structure characterization of Middle East carbonates. J. Petr. Sci. Eng., 146, 570–583. https://doi.org/10.1016/j.petrol.2016.07.018
Hoerlle, F.O., Silva, W.G.A.L., Pontedeiro, E.M., Couto, P., 2020. Porous system characterization of a heterogeneous carbonate rock bed using x-ray microtomography. In: Interpore. Qingdao, China.
Jia, B., 2019. Carbonated water injection (CWI) for improved oil recovery and carbon storage in high-salinity carbonate reservoir. J. Taiwan Inst. Chem. Eng., 104, 82–93.
Kantzas, A., Bryan, J., Taheri, S., 2012. Fundamentals of Fluid Flow in Porous Media. Open Source https://perminc.com /resources/fundamentals-of-fluid-flow-in-porous-media/
Lima, M.C.O., Pontedeiro, E.M., Ramirez, M.G., Boyd, A., van Genuchten, M.Th., Borghi, L.F., Couto, P., Raoof, A., 2020. Petrophysical correlations for permeability of coquinas (carbonate rocks). Transp. Porous Media, 135, 287–308. https://doi.org/10.1007/ s11242-020-01474-1
Luquot, L., Rodriguez, O., Gouze, P., 2014. Experimental characterization of porosity structure and transport property changes in limestone undergoing different dissolution regimes. Transp. Porous Media, 101, 3, 507–532.
Mahzari, P., Jones, A.P., Oelkers, E.H., 2019. An integrated evaluation of enhanced oil recovery and geochemical processes for carbonated water injection in carbonate rocks. J. Petr. Sci. Eng., 181, 106188.
Mazzullo, S.J., 2004. Overview of porosity in carbonate reservoirs. Kansas Geol. Soc. Bull., 79, 1–2, 1–19.
Meiboom, S., Gill, D., 1958. Modified spin-echo method for measuring nuclear relaxation times. Rev. Scient. Instr., 29, 688. https://doi.org/10.1063/1.1716296
Menke, H.P., Andrew, M.G., Blunt, M.J., Bijeljic, B., 2016. Reservoir condition imaging of reactive transport in heterogeneous carbonates using fast synchrotron tomography; Effect of initial pore structure and flow conditions. Chem. Geol., 428, 15–26.
Molins, S., Trebotich, D., Yang, L., Ajo-Franklin, J.B., Ligocki, T.J., Shen, C., Steefel, C., 2014. Pore-scale controls on calcite dissolution rates from flow-through laboratory and numerical experiments. Env. Sci. Techn., 48, 13, 7453–7460. DOI: 10.1021/es5013438
Nowrouzi, I., Manshad, A.K., Mohammadi, A.H., 2020. The mutual effects of injected fluid and rock during imbibition in the process of low and high salinity carbonated water injection into carbonate oil reservoirs. J. Molec. Liq., 305, 112432.
Oliveira, J.A.T., Cássaro, F.A.M., Pires, L.F., 2020. The porous size distribution obtained and analyzed by free access software. Revista Brasileira de Ensino de Física, 42.
Paraview, 2020. Paraview version 5.9.0. Kitware.
PoreStudio, 2021. PoreStudio. https://porestudio.com
Prodanović, M., Lindquist, W.B., Seright, R.S., 2004. 3D microtomographic study of fluid displacement in rock cores. Devel. Water Sci., 55, 1, 223–234. DOI: 10.1016/S0167-5648(04)80052-2
Ramamoorthy, R., Boyd, A., Neville, T., Seleznev, N., Sun, H., Flaum, C., Ma, J., 2008. A new workflow for petrophysical and textural evaluation of carbonate reservoirs. In: Proc. SPWLA 49th Annual Logging Symposium.
Rabbani, A., Babaei, M., 2019. Hybrid pore-network and Lattice-Boltzmann permeability modelling accelerated by machine learning. Adv. Water Resour., 126, 116–128. DOI: 10.1016/j.advwatres.2019.02.012
Raoof, A., Hassanizadeh, S.M., 2012. A new formulation for pore- network modeling of two- phase flow. Water Resour. Res., 48, 1. https://doi.org/10.1029/2010WR010180
Raoof, A., Nick, H.M., Hassanizadeh, S.M., Spiers, C.J., 2013. PoreFlow: a complex pore network model for simulation of reactive transport in variably saturated porous media. Comp. Geosci., 61, 160–174.
Rocha, A.S., Pontedeiro, E.M. B.D., Alves, J.L.D., Silva, W.G.A.L., 2019. Obtaining pore-size distribution by image analysis of stacks with large image spacing without resizing. In: CILAMCE 2019, XL Ibero-Latin-American Congress on Computational Methods in Engineering.
Saxena, N., Hofmann, R., Alpak, F.O., Berg, S., Dietderich, J., Agarwal, U., Tandon, K., Hunter, S., Freeman, J., Wilson, O.B., 2017. References and benchmarks for pore-scale flow simulated using micro-CT images of porous media and digital rocks. Adv. Water Resour., 109, 211–235. https://doi.org/10.1016/j.advwatres.2017.09.007
Schafer, W., 1972. Ecology and Paleoecology of Marine Environments. Univ. Chicago Press, Chicago, 568 p.
Schnaar, G., Brusseau, M.L., 2006. Characterizing pore-scale configuration of organic immiscible liquid in multiphase systems with synchrotron X-ray microtomography. Vadose Zone J., 5, 2, 641–648. http://dx.doi.org/10.2136/vzj2005.0063
Seyyedi, M., Mahmud, H.K.B., Verral, M., Giwelli, A., Esteban, L., Ghasemiziarani, M., Clennell, B., 2020. Pore structure changes occur during CO_2 injection into carbonate reservoirs. Scientific Reports, 10, 3624.
Sheng, J.J., 2013. Enhanced oil recovery field case studies. Gulf Professional Publishing.
Yang, Z., Peng, X.F., Lee, D.J., Chen, M.Y., 2009. An image-based method for obtaining pore-size distribution of porous media. Env. Sci. Techn., 43, 9, 3248–3253.
Thompson, D.L., Stilwell, J.D., Hall, M., 2015. Lacustrine carbonate reservoirs from early Cretaceous Rift Lakes of Western Gondwana: Pre-salt Coquinas of Brazil and West Africa. Gondwana Res., 28, 1, 26–51. http://dx.doi.org/10.1016/j.gr.2014.12.005
Wang, Q., Yang, S., Han, H., Wang, L., Qian, K., Pang, J., 2019. Experimental investigation on the effects of CO_2 displacement methods on petrophysical property changes of ultra-low permeability sandstone reservoirs near injection wells. Energies, 12, 327–347.
Wilson, A., 2014. Multiscale simulation of WAG flooding in naturally fractured reservoirs. J. Petr. Techn., 66, 73–75. https://doi.org/10.2118/0114-0073-JPT

Received 1 October 2021
Accepted 27 December 2021